2026 IEEE International Conference on Robotics and Automation (ICRA 2026)
June 1-5, 2026. Vienna, Austria

A Whole-Body Control Framework for Human-like Walking with Knee Stretch on Flat-Foot Humanoids

Taehyun Kim[1,2], Sookyoung Yoo[1,2], Myo-Taeg Lim[2] and Yonghwan Oh[1,*]

***Abstract*— Achieving a natural, human-like heel to toe gait on flat-foot humanoids is a challenging task, as their typical parallel foot walking pattern limits step length and appears unnatural. To address this, we present a hierarchical control framework guided by a four-state Finite State Machine with mixed time and event based transitions. The controller manages near-singular knee extension using a 5-DoF damped least squares inverse kinematics task for the swing leg. A key innovation is a late-swing ankle policy based on the shank-to-vertical angle, which allows a natural heel strike to emerge and adapt to walking speed. A real-time whole-body controller based on quadratic programming, incorporating the robot's full-body dynamics, realizes these motions while satisfying contact constraints. In simulation, our method achieves significantly longer steps with maintained stability and reduced stance knee effort, reaching a maximum step length of 72 cm (39.6% of the robot's height), which is comparable to that of a human.**

I. Introduction

Humanoid locomotion has made significant progress in achieving stable walking, yet replicating the natural human gait remains a challenging task. This lack of naturalness is evident in several characteristic aspects of humanoid walking. The most prominent problem is a gait with continuously bent knees, where the legs never fully extend. This posture, strategy to avoid kinematic singularities, is also a primary cause of high energy consumption [1]. Furthermore, as shown in Fig. 1(a), the swing leg is typically maintained in a horizontal posture relative to the ground. While effective for ensuring stability, these strategies create a fundamentally restrictive gait. The resulting motion is not only visibly unnatural but also limits the robot's ability to take long strides. Such a restrictive gait directly prevents it from matching the performance of a typical human, whose step length can reach up to 40% of their body height [2].

In contrast, human walking follows a heel to toe pattern in which the foot first contacts the ground with the heel, then moves into a foot-flat stance before concluding with a toe off [3] as illustrated in Fig. 1(b). This rolling motion is key to achieving long, efficient strides. To replicate this natural gait, several studies have investigated walking on humanoids that incorporate actuated toe joints. WABIAN, for example, was retrofitted with an active toe joint and controlled through inverse kinematics (IK) to realize heel to toe transitions and step lengths up to 50cm [4]. Likewise, simulation studies on Atlas used an active toe joint combined with quadratic-programming (QP) based dynamic control to realize heel to toe walking with 50cm steps [5]. These modifications not only extended step length but also lowered energy consumption during walking [6], [7]. However, such solutions require actuated toe joints and are therefore not applicable to the majority of humanoids that feature flat foot. Furthermore, their reliance on predefined joint angle trajectories prevents adaptation to varying walking speeds, resulting in rigid and unnatural gait. This is particularly problematic because most humanoids [8]–[13] feature flat, rectangular foot without toe joints for structural simplicity. For these robots, reproducing heel strike and toe off remains challenging. [14] presents a hybrid approach that enables underactuated heel off and toe support by coordinating virtual force control on the stance leg and foot placement on the swing leg, structuring the gait into three phases. However, omitting friction cone force constraints, which can compromise stability, and models each leg with only 3 degrees of freedom (DOF), oversimplifying the robot's kinematics. More recently, [15] divides heel to toe walking into a four state finite state machine (FSM) that relies on time based transitions. Joint angles are computed through QP and then tracked with IK. However, the segmented phases do not fully capture human gait, and the use of fixed timing and IK without dynamic consistency often results in discontinuous,

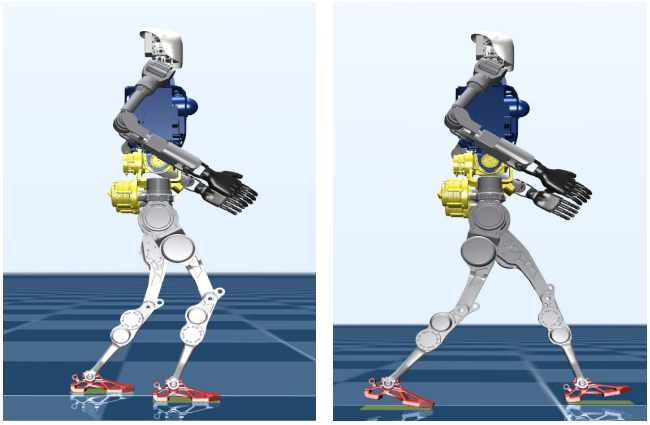

(a) Flat-foot walking (b) Heel to toe walking

Fig. 1. **Flat-foot and heel to toe walking** (a) Flat-foot walking with the swing foot kept nearly horizontal to the ground. (b) Heel to toe walking with heel strike and heel off, enabling longer steps.

*This work was supported by the Korea Institute of Science and Technology Institutional Programs under grant numbers 2MRF970. The center for humanoid research, Korea Institute of Science and Technology (KIST), Seoul, 136-791, Republic of Korea.

[1]The center for Intelligent Interactive Robotics, Korea Institute of Science and Technology (KIST), Seoul, 136-791, Republic of Korea. {xogus226, zkxm0112, oyh}@kist.re.kr

[2]School of Electrical Engineering, Korea University, Seoul 02841, South Korea. {2024020815, skyoo, mlim}@korea.ac.kr

contact-inconsistent motion. [16] employs a passivity-based whole body controller to generate a heel-off motion and achieves step lengths of about 55 cm (31.6 % of its height). Because the gait omits a heel strike phase it remains less natural and is limited to a slow 1.5 s step cycle.

To address these limitations, this paper presents a new hierarchical framework for achieving a natural heel to toe gait on flat foot humanoids. Our approach is guided by a four-state FSM that integrates both time based and event triggered transitions to better reflect human gait characteristics. At the high level, a swing leg controller uses damped least squares (DLS) IK to avoid singularity issues, while ankle policy based on the shank-to-vertical angle allows a natural heel strike to emerge as walking speed increases. At the low level, a real-time whole-body controller enforces appropriate contact constraints for each gait phase. Through this framework, we demonstrate a smoother, more human-like gait with significantly longer steps and reduced knee effort.

In the sections that follow, Section II establishes a kinematic upper bound on step length under heel to toe rollover. Section III then introduces the FSM that blends time and event based transitions. Section IV presents a DLS swing-leg inverse kinematics to handle knee stretch and explains the ankle-pitch joint command strategy. Section V details the QP whole-body controller with phase-specific contact constraints. Section VI presents simulation results, and Section VII summarizes our findings.

II. Kinematic Advantages of Heel to Toe Walking over Flat-Foot Walking

This section derives a kinematic upper bound on the maximum step length for flat-foot walking and heel to toe walking, under the same pelvis height h. Fig. 2 illustrates a planar 3-link leg (thigh ℓ_1, shank ℓ_2).

(a) Flat-foot walking: When the foot remains parallel to the ground, the ankle acts as a fixed pivot. At full knee extension (overall leg length $\ell_1 + \ell_2$), the horizontal projection from pelvis to contact is

$$x_{\text{flat}} = \sqrt{(\ell_1 + \ell_2)^2 - h^2}, \qquad 0 < h < \ell_1 + \ell_2, \quad (1)$$

so the symmetric maximum step length is

$$L_{\max}^{\text{flat}} = 2\sqrt{(\ell_1 + \ell_2)^2 - h^2}. \quad (2)$$

(b) Heel to toe walking: During heel to toe walking the supporting foot rotates about a moving pivot. Unlike flat-foot gait the foot can keep a nonzero pitch so the ground pivot shifts with the foot. Let ℓ_{t} and ℓ_{h} be the ankle-to-pivot distances on the toe and heel sides. With the knee fully extended the pelvis to pivot horizontal projections are

$$\begin{aligned} x_{\text{t}} &= \sqrt{(\ell_1 + \ell_2)^2 - \left(h - \ell_{\text{t}} \sin\theta_1\right)^2} \\ x_{\text{h}} &= \sqrt{(\ell_1 + \ell_2)^2 - \left(h - \ell_{\text{h}} \sin\theta_2\right)^2}. \end{aligned} \quad (3)$$

and the maximum step length becomes

$$L_{\max}^{\text{heel–toe}} = x_{\text{t}} + x_{\text{h}}. \quad (4)$$

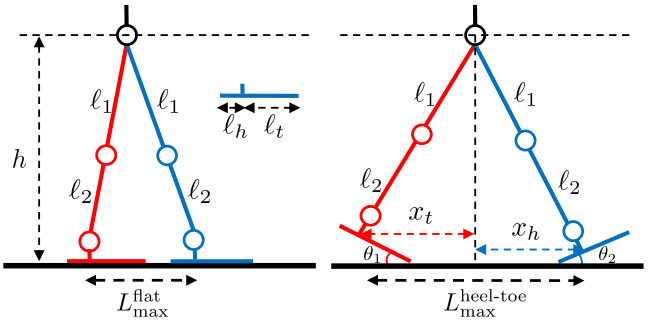

(a) Flat-foot walking (b) Heel to toe walking

Fig. 2. **Maximum step length with and without heel to toe rollover (planar 3-link model).** (a) Flat-foot walking with rotation about the ankle, which limits $L_{\max}^{\text{flat}}$. (b) Heel to toe rollover where heel-rise angles θ_1 and θ_2 move the ground-contact location forward from the heel edge by x_h toward the toe edge by x_t, increasing $L_{\max}^{\text{heel-toe}}$.

For heel rise angles $\theta_1, \theta_2 \in [0, \frac{\pi}{2}]$,

$$L_{\max}^{\text{heel–toe}} = x_{\text{t}} + x_{\text{h}} \;\geq\; 2\sqrt{(\ell_1 + \ell_2)^2 - h^2} = L_{\max}^{\text{flat}}. \quad (5)$$

with strict inequality whenever at least one of θ_1, θ_2 is nonzero. Therefore $L_{\max}^{\text{heel–toe}}$ increases monotonically as θ_1 and θ_2 increase over the practical range (where $\ell_{\text{t}} \sin\theta_1$, $\ell_{\text{h}} \sin\theta_2 < h$), and it reduces continuously to (2) when $\theta_1 = \theta_2 = 0$.

III. Flat Foot Humanoid's Gait Cycle Analysis

We introduce a FSM for implementing a heel to toe walking on flat foot humanoid systems. We then detail each contact state and explain the transition mechanisms triggered by time and by events.

A. Flat foot humanoid FSM for Heel to Toe walking

In conventional flat foot walking, the foot remains parallel to the ground throughout the gait cycle, preventing natural heel to toe transitions. To further achieve a human-like gait, we subdivide the walking cycle into four state FSM for the contact phase.

i) Heel Strike(=Toe off): This phase marks the initial ground contact of the swinging foot's heel. Concurrently, the support foot has already completed its heel contact phase and initiates a heel rise.

ii) Loading Response: Following Heel strike, the transition from heel contact to sole contact occurs through a natural roll over process. During this phase, the supporting foot achieves toe contact, just before entering its swing phase.

iii) Midstance: The support foot maintains complete plantar contact with the ground to securely stabilize the body's weight. Concurrently, the swinging foot advances to prepare for the subsequent step.

iv) Heel Off: After Midstance, the support foot undergoes a gradual heel lift off. This critical phase of natural roll over facilitates the smooth transition of the support foot into the swing phase.

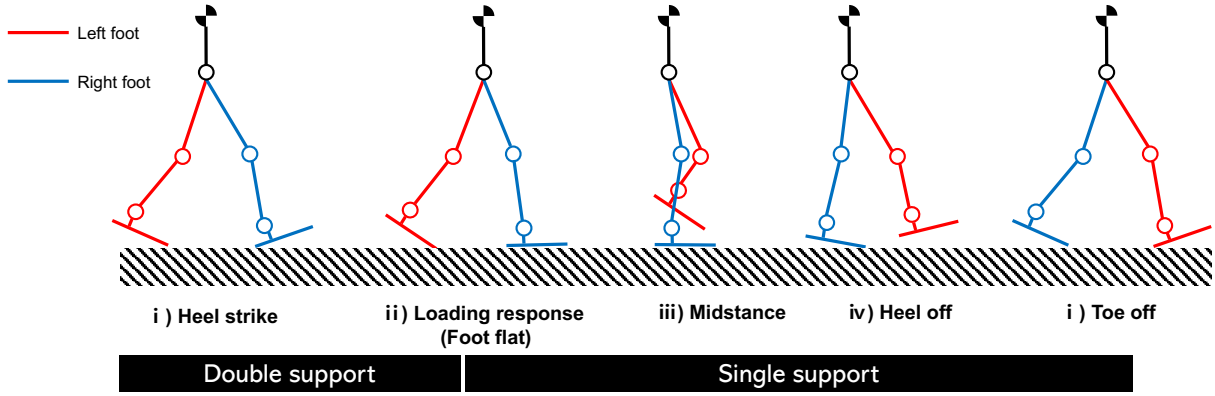

Fig. 3. **Finite State Machine for flat foot humanoid heel to toe walking.** The diagram includes four contact states— Heel Strike(Toe off), Loading Response, Midstance, and Heel Off. Transitions are driven by a combination of predefined timings and kinematic events to replicate the natural human gait cycle.

B. Gait Phase Transition Timing and Trigger Mechanisms

To implement natural gait transitions similar to human walking, our system combines the FSM with both time based and event based triggers. (Loading response) $\rightarrow$ (Midstance) and (Heel off) $\rightarrow$ (Toe off) follow the footstep planner's schedule. All other transitions are driven by dedicated triggers described below. We employ two types of transition mechanisms. The first is (Heel strike) $\rightarrow$ (Loading response) and it is time based. In human gait Heel strike and the subsequent Loading response occur at the start of double support and swing begins shortly after [3]. To reflect this timing, our planner allocates 80% of the predetermined double stance duration to the Heel strike phase and the remaining 20% to the Loading response phase. The second transition occurs when the robot moves from (Midstance) $\rightarrow$ (Heel off). We trigger this event as soon as the CoM has passed the front edge of the support foot. Passing this boundary shows that the robot's weight has shifted forward enough to lift the heel. This event based approach enables the system to promptly adapt to changes in the walking environment or speed, thereby enabling more flexible FSM transitions. Such an event based trigger mechanism effectively captures the dynamic characteristics of the gait cycle, contributing significantly to the implementation of natural gait transitions compared to a purely time based method.

C. Knee Stretch in the FSM

We focus on knee stretch that can arise in both the stance and swing legs within the FSM. First, after Loading response, when the supporting foot initiates swing, the knee of that foot may become nearly fully extended, which can lead to a singularity issue. Second, during Heel off, as the body progresses in the direction of motion, the supporting leg's knee also straightens, which can lead to a singularity issue. In optimization, such singular conditions can result in no feasible solution, which in turn can cause the robot to diverge. In the following section, we introduce our heel to toe whole body control that addresses these issues.

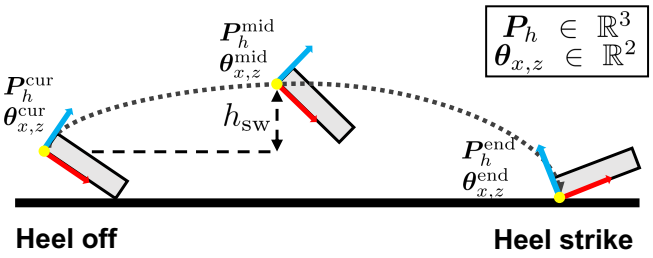

Fig. 4. **Swing foot trajectory from Heel off to Heel strike phase.** The path is generated via cubic spline interpolation through predefined midpoint, and end waypoints.

IV. Swing Foot Trajectory and Damped Least Squares IK for Heel to Toe Walking

A. Swing Foot Trajectory in the Heel Frame

To generate the task-space reference we parameterize the swing motion at the heel frame rather than the foot center (Fig. 4). Let $\boldsymbol{p}_h(t) \in \mathbb{R}^3$ be the heel position and let $\boldsymbol{\theta}_{xz}(t) \in \mathbb{R}^2$ collect roll and yaw (pitch is intentionally left unconstrained by the 5-DoF task). The trajectory is a cubic spline through start, mid, and end waypoints:

$$\boldsymbol{p}_h^{\text{mid}} = \begin{bmatrix} \frac{1}{2}\left(p_{h,x}^{\text{cur}} + p_{h,x}^{\text{end}}\right) \\ \frac{1}{2}\left(p_{h,y}^{\text{cur}} + p_{h,y}^{\text{end}}\right) \\ p_{h,z}^{\text{cur}} + h_{\text{sw}} \end{bmatrix}. \tag{6}$$

where $h_{\text{sw}} > 0$ is the prescribed swing height. On level ground we set

$$p_{h,z}^{\text{end}} = 0, \tag{7}$$

and choose roll and yaw waypoints to keep the foot neutral about both axes:

$$\boldsymbol{\theta}_{xz}^{\text{cur}} = \text{xz}\left(\boldsymbol{R}_h(t_s)\right), \quad \boldsymbol{\theta}_{xz}^{\text{mid}} = \mathbf{0}, \quad \boldsymbol{\theta}_{xz}^{\text{end}} = \mathbf{0}, \tag{8}$$

where t_s and t_f denote the swing start and touch-down times, respectively, and the function $\text{xz}(\cdot)$ extracts the roll and yaw angles from the rotation matrix $\boldsymbol{R}_h$. Each component of $(\boldsymbol{p}_h(t), \boldsymbol{\theta}_{xz}(t))$ and $(\dot{\boldsymbol{p}}_h(t), \dot{\boldsymbol{\theta}}_{xz}(t))$ is obtained from a cubic

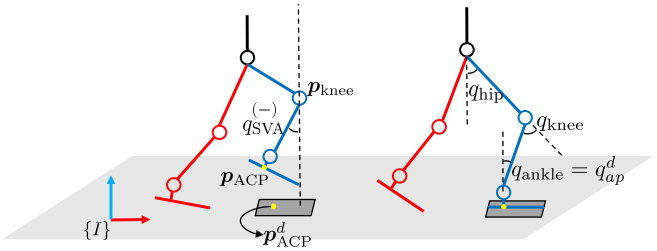

Fig. 5. **Flat landing preparation in late swing.** Negative SVA predicts a flat landing.

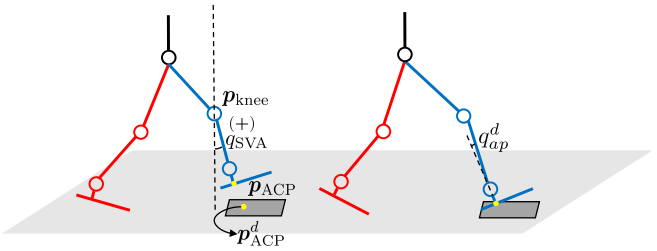

Fig. 6. **Heel strike preparation in late swing.** Positive SVA triggers heel-first landing.

spline that enforces position and velocity continuity at the waypoints. We use the measured heel velocity at lift-off and impose zero terminal velocity at touch-down.

$$\dot{\boldsymbol{p}}_h(t_s) = \dot{\boldsymbol{p}}_h^{\text{cur}}, \qquad \dot{\boldsymbol{p}}_h(t_f) = \boldsymbol{0}. \tag{9}$$

This heel frame parameterization has two practical advantages: (i) Setting the mid-swing height $p^{\text{mid}}_{h,z} = p^{\text{cur}}_{h,z} + h_{\text{sw}}$ ensures adequate toe clearance throughout swing without explicitly computing a heel-rise angle. (ii) On flat terrain, setting $p^{\text{end}}_{h,z} = 0$ yields a flat-foot landing without estimating a heel-strike angle.

B. Ankle-Pitch Command for Heel to Toe Gait

Swing-foot Cartesian task uses only five DoFs, we command the remaining DoF (ankle pitch) in joint space. Let the elapsed swing time be

$$t_{\text{sw}} := t - t_s \in [0, T_{\text{sw}}], \qquad T_{\text{sw}} := t_f - t_s,$$

and let the onset of late swing be $t_{\text{late}} := \alpha\, T_{\text{sw}}$ with $\alpha \approx 0.67$. This value is chosen from normative gait timing and corresponds to the terminal–swing phase of normal gait [3].

Early swing ($0 \le t_{\text{sw}} < t_{\text{late}}$)*:* The ankle is biased toward neutral to reduce toe drag and match human swing posture:

$$q^d_{ap}(t) = 0. \tag{10}$$

Late swing ($t_{\text{sw}} \ge t_{\text{late}}$)*:* We decide ahead of time using the Shank-to-Vertical Angle (SVA), defined as the angle between the shank (tibia) axis and the global vertical. Near late swing, we compare the forward knee position $p_{\text{knee},x}(t)$ with the desired ankle–contact point on the foot sole $p^d_{\text{ACP},x}$. The sign of SVA is predicted by

$$\text{sgn}\left(q_{\text{SVA}}\right) \;=\; \text{sgn}\left(p^d_{\text{ACP},x} - p_{\text{knee},x}\right). \tag{11}$$

When the step length is short or the knee remains markedly bent, it is often the case that $p_{\text{knee},x} > p^d_{\text{ACP},x}$, yielding $q_{\text{SVA}} < 0$; in this case a heel strike would be unnatural and the foot should land flat (see Fig. 5). For a flat landing the foot is parallel to the ground when

$$q_{\text{hip}} + q_{\text{knee}} + q_{\text{ankle}} = 0, \tag{12}$$

which yields the ankle-pitch reference

$$q^d_{ap} = -(q_{\text{hip}} + q_{\text{knee}}). \tag{13}$$

Conversely, when the planned step is sufficiently long so that $p^d_{\text{ACP},x} > p_{\text{knee},x}$, we obtain $q_{\text{SVA}} > 0$; the shank is tipped forward and a heel strike is kinematically appropriate (see Fig. 6). In this case we prescribe a near neutral, slightly dorsiflexed ankle angle at initial contact by setting

$$q^d_{ap} = K, \tag{14}$$

with $K \approx 0.1$ rad ($\approx 6^\circ$ dorsiflexion), consistent with normative ankle posture at heel strike in human gait [17]. In practice, this fixed setpoint naturally produces a heel strike, and no explicit specification or tuning of the heel–ground strike angle is required. The ankle-pitch acceleration command is generated by a joint acceleration PD law:

$$\ddot{q}^{\text{cmd}}_{ap} = K_{ap,p}\big(q^d_{ap} - q_{ap}\big) + K_{ap,d}\big(0 - \dot{q}_{ap}\big). \tag{15}$$

C. Swing-Foot IK with Damped Least Squares

As discussed in Sec. III-C, large step lengths tend to push the swing leg toward full knee extension, where the swing-leg Jacobian becomes ill-conditioned and a full 6-DoF Cartesian task loses authority. To keep tracking robust in these configurations, we regulate the swing foot with a 5-DoF Cartesian task (position + roll/yaw) using acceleration-level DLS-IK. Let the desired Cartesian acceleration be

$$\ddot{\boldsymbol{X}}^{ref}_{\text{sw},5} = \left[\left(\ddot{\boldsymbol{p}}^{ref}_{\text{sw}}\right)^\top \;\; \left(\dot{\boldsymbol{\omega}}^{ref}_{\text{sw}}\right)^\top\right]^\top, \tag{16}$$

with $\ddot{\boldsymbol{p}}^{ref}_{\text{sw}} \in \mathbb{R}^3$ and $\dot{\boldsymbol{\omega}}^{ref}_{\text{sw}} \in \mathbb{R}^2$ constructed exactly as in

$$\ddot{\boldsymbol{p}}^{ref}_{\text{sw}} = \ddot{\boldsymbol{p}}^d_h + \boldsymbol{K}_p(\boldsymbol{p}^d_h - \boldsymbol{p}_h) + \boldsymbol{K}_d(\dot{\boldsymbol{p}}^d_h - \dot{\boldsymbol{p}}_h), \tag{17}$$

$$\dot{\boldsymbol{\omega}}^{ref}_{\text{sw}} = \dot{\boldsymbol{\omega}}^d_h + \boldsymbol{K}_p \log(\boldsymbol{R}^d_h \boldsymbol{R}^T_h) + \boldsymbol{K}_d(\boldsymbol{\omega}^d_h - \boldsymbol{\omega}_h). \tag{18}$$

$\boldsymbol{R}_h$ is the current heel frame's orientation matrices. The gains $\boldsymbol{K}_p$ and $\boldsymbol{K}_d$ are the proportional and derivative feedback gains, while the operator $\log(\cdot)$ computes the matrix logarithm. $\ddot{\boldsymbol{p}}^d_h$ and $\dot{\boldsymbol{\omega}}^d_h$ are taken from the spline's analytic derivative. We regulate only roll and yaw in orientation, leaving pitch free. Define

$$\boldsymbol{S}_5 = \begin{bmatrix} \boldsymbol{I}_3 & \boldsymbol{0} \\ \boldsymbol{0} & \boldsymbol{E}_{xz} \end{bmatrix}, \qquad \boldsymbol{E}_{xz} = \begin{bmatrix} 1 & 0 & 0 \\ 0 & 0 & 1 \end{bmatrix}. \tag{19}$$

With the swing-leg Jacobian $\boldsymbol{J}_{\text{sw}} \in \mathbb{R}^{6\times 6}$ and its time derivative $\dot{\boldsymbol{J}}_{\text{sw}}$, define the 5-DoF task reduction:

$$\boldsymbol{J}_{\text{sw},5} = \boldsymbol{S}_5\, \boldsymbol{J}_{\text{sw}}, \qquad \dot{\boldsymbol{J}}_{\text{sw},5} = \boldsymbol{S}_5\, \dot{\boldsymbol{J}}_{\text{sw}}. \tag{20}$$

The desired swing joint acceleration is then

$$\ddot{\boldsymbol{q}}^{\text{sw}}_d = \left(\boldsymbol{J}_{\text{sw},5}\right)^{\#_\lambda} \left(\ddot{\boldsymbol{X}}^{ref}_{\text{sw},5} - \dot{\boldsymbol{J}}_{\text{sw},5}\, \dot{\boldsymbol{\xi}}_{\text{sw}}\right), \tag{21}$$

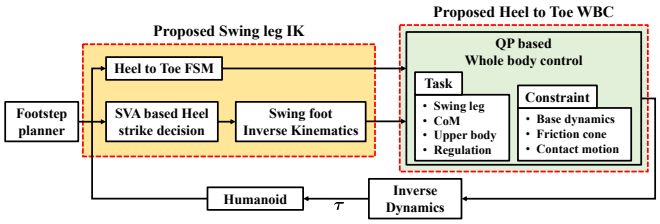

Fig. 7. Overview of the proposed hierarchical heel to toe walking framework. The system consists of a high-level swing leg IK module with an SVA-based landing policy and a low-level QP-based whole body controller.

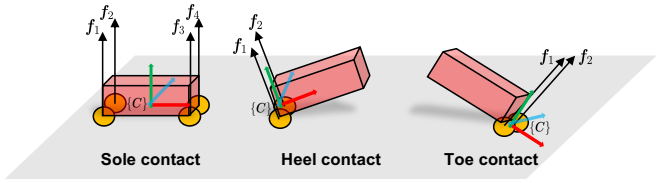

Fig. 8. Three contact types that can occur in flat foot. $\{\boldsymbol{C}\}$ denotes the contact frame, and the orange circle indicates the contact point.

where $\dot{\boldsymbol{\xi}}_{\text{sw}} \in \mathbb{R}^6$ denotes the joint velocity vector of the swing leg. The damped least squares pseudoinverse is defined as

$$\left(\boldsymbol{J}_{\text{sw},5}\right)^{\#_\lambda} = \boldsymbol{J}_{\text{sw},5}^{\top}\left(\boldsymbol{J}_{\text{sw},5}\boldsymbol{J}_{\text{sw},5}^{\top} + \lambda^2 \boldsymbol{I}_5\right)^{-1}. \tag{22}$$

V. QP-Based Heel to Toe Walking Whole Body Controller

In this section, we describe a whole body controller(WBC) that utilizes quadratic programming. The controller implements the FSM defined in Section III to achieve human-like walking in flat foot humanoids. The overall architecture of the proposed control framework is illustrated in Fig. 7, showcasing the hierarchical integration of the swing leg IK and the QP-based WBC.

A. QP Variables for Contact Scenarios

To solve the QP problem, we must define the decision variables, which vary according to the number of ground contacts determined by our FSM. Fig. 8 illustrates the classification of contact cases generated by the FSM employed in this study. There are three distinct contact scenarios in total. In the case of a sole contact, a surface contact is established, which requires solving for four force vectors $\boldsymbol{f}$ (one for each vertex). For the heel contact and toe contact cases, a line contact occurs, and only two force vectors $\boldsymbol{f}$ are solved. Therefore, the decision variables used for WBC are as follows.

$$\boldsymbol{X} = \begin{bmatrix} \ddot{\boldsymbol{\xi}} \\ \boldsymbol{f}_{n_c} \end{bmatrix}. \tag{23}$$

where $\ddot{\boldsymbol{\xi}} \in \mathbb{R}^{6+n}$ denotes the joint accelerations. $\boldsymbol{f}_{n_c}$ represents the contact force, with n_c indicating the number of contact forces to be solved. Additionally, $\boldsymbol{f}$ refers to the force components f_x, f_y and f_z

B. Task Formulation for QP Based Heel to Toe Walking

We present the multiple tasks and constraints required to implement a WBC for heel to toe walking using QP.

1) CoM tracking: We regulate the CoM position and base orientation with a force-based formulation built on a Single Rigid Body Dynamics approximation. We define the cost function for CoM control as follows:

$$L_{CoM} = \|\boldsymbol{A}_{CoM}\boldsymbol{X} - \begin{bmatrix}\boldsymbol{f}^{ref} & \boldsymbol{\mu}^{ref}\end{bmatrix}^T\|^2_{\boldsymbol{W}_{CoM}}, \tag{24}$$

where the matrix $\boldsymbol{A}_{CoM}$ is given by

$$\boldsymbol{A}_{CoM} = \begin{bmatrix} \boldsymbol{0}_{3\times(6+n)} & \boldsymbol{I} & \cdots & \boldsymbol{I} \\ \boldsymbol{0}_{3\times(6+n)} & \boldsymbol{S}(\boldsymbol{r}_1) & \cdots & \boldsymbol{S}(\boldsymbol{r}_{n_c}) \end{bmatrix}. \tag{25}$$

In these expressions, L_{CoM} is the cost function weighted by $\boldsymbol{W}_{CoM}$, and $\boldsymbol{I}$ is the identity matrix. The operator $\boldsymbol{S}(\cdot)$ represents the skew-symmetric matrix corresponding to the vector. Furthermore, $\boldsymbol{r}_{n_c}$ denotes the distance from the CoM to the ground contact point. The reference force $\boldsymbol{f}^{ref}$ and reference moment $\boldsymbol{\mu}^{ref}$ are computed as

$$\boldsymbol{f}^{ref} = m(\ddot{\boldsymbol{p}}_G^{ref} + \boldsymbol{g}), \tag{26}$$

$$\boldsymbol{\mu}^{ref} = \boldsymbol{I}_G\dot{\boldsymbol{w}}_b^{ref} + \boldsymbol{S}(\boldsymbol{w}_b^d)\boldsymbol{I}_G\boldsymbol{w}_b^d. \tag{27}$$

Here, m is the robot's total mass, $\boldsymbol{g}$ is the gravitational acceleration, and $\ddot{\boldsymbol{p}}_G^{ref}$ represents the reference acceleration of CoM. The matrix $\boldsymbol{I}_G$ is centroidal rotational inertia, $\boldsymbol{\omega}_b$ is the current base angular velocity. The reference CoM and base angular accelerations are formulated as feedback, in the same manner as (17) and (18).

2) Swing-foot joint tracking: Tracking of the 5-DoF IK target (Sec. IV-C) and the ankle-pitch policy (Sec. IV-B) is encoded in the QP by the quadratic term

$$L_{sw} = \left\| \boldsymbol{S}_{\text{sw}}\ddot{\boldsymbol{\xi}} - \ddot{\boldsymbol{q}}_{\text{sw}}^d \right\|^2_{\boldsymbol{W}_{\text{sw-IK}}} + \left\| \boldsymbol{S}_{ap}\ddot{\boldsymbol{\xi}} - \ddot{q}_{ap}^d \right\|^2_{\boldsymbol{W}_{ap}}, \tag{28}$$

where $\boldsymbol{S}_{\text{sw}}$ selects the six swing-leg joints and $\boldsymbol{S}_{ap}$ selects the ankle-pitch joint. The references $\ddot{\boldsymbol{q}}_{\text{sw}}^d$ and $\ddot{q}_{ap}^d$ are provided by the DLS-IK and the early/late-swing ankle policy, respectively.

3) Upper body motion: In redundant humanoid systems, unconstrained upper-body joints can produce undesired movements that compromise walking stability, so we fix the upper-body posture.

$$L_{up} = \|\boldsymbol{S}_{up}\boldsymbol{X} - \ddot{\boldsymbol{\xi}}_{up}^{ref}\|^2_{\boldsymbol{W}_{up}}, \tag{29}$$

where

$$\ddot{\boldsymbol{\xi}}_{up}^{ref} = \boldsymbol{K}_p(\boldsymbol{\xi}_{up}^d - \boldsymbol{\xi}_{up}) - \boldsymbol{K}_d\dot{\boldsymbol{\xi}}_{up}. \tag{30}$$

The matrix $\boldsymbol{S}_{up}$ selects the upper-body joints, and $\ddot{\boldsymbol{\xi}}_{up}^{ref}$ is generated using a PD servo.

4) Regularization: The regularization term ensures a unique solution and enhances numerical stability. It also constrains the magnitude of contact forces and joint accelerations, preventing abrupt command outputs and promoting smoother robot motion.

$$L_{reg} = \|\boldsymbol{X}\|^2_{\boldsymbol{W}_{reg}}. \tag{31}$$

C. Constraint Definitions

As shown in Fig. 8, there are three types of contacts. We describe the required constraints for each contact type.

1) Sole contact: For sole contact, the foot must remain fixed relative to the ground. Therefore, six acceleration equality constraints are defined.

$$\begin{aligned} \ddot{\boldsymbol{X}}_c &= \boldsymbol{J}_c\ddot{\boldsymbol{\xi}} + \dot{\boldsymbol{J}}_c\dot{\boldsymbol{\xi}} = \boldsymbol{0}, \\ \ddot{\boldsymbol{X}}_c &= \left[\ddot{p}_x, \ddot{p}_y, \ddot{p}_z, \dot{\omega}_x, \dot{\omega}_y, \dot{\omega}_z\right]^T. \end{aligned} \tag{32}$$

where $\boldsymbol{J}_c$ denotes the Jacobian of the contact frame. $\ddot{\boldsymbol{p}}$ and $\dot{\boldsymbol{\omega}}$ denote the linear and angular accelerations, respectively.

2) Heel contact, Toe contact: Line contact occurs during either heel contact or toe contact. In a line contact, the contact Jacobian loses one rotational constraint about the contact line, so only five independent constraints are physically enforceable (rank 5) [18]. We therefore constrain three translations and two rotations (roll and yaw), while leaving pitch unconstrained so that the foot can rock about the contact line and achieve a smooth transition from Heel strike to Loading response without over-constraining.

$$\begin{aligned} \ddot{\boldsymbol{X}}_c &= \boldsymbol{J}_c\ddot{\boldsymbol{\xi}} + \dot{\boldsymbol{J}}_c\dot{\boldsymbol{\xi}} = \boldsymbol{0}, \\ \ddot{\boldsymbol{X}}_c &= \left[\ddot{p}_x, \ddot{p}_y, \ddot{p}_z, \dot{\omega}_x, \dot{\omega}_z\right]^T. \end{aligned} \tag{33}$$

With the stance foot in line contact, no singularity arises even at full knee extension because only five constraints are enforced. The contact Jacobian becomes ill-conditioned mainly along foot pitch, which is left free, so the selected contact Jacobian retains rank 5 and the QP remains feasible.

D. QP based Whole Body Controller

QP solves a quadratic cost under linear equality and inequality constraints, enabling efficient real time whole body control. At each control step, we solve

$$\begin{aligned} \min_{\ddot{\boldsymbol{\xi}}, \boldsymbol{f}_{n_c}} \quad & L_{CoM} + L_{sw} + L_{up} + L_{reg} \\ \text{subject to} \quad & \ddot{\boldsymbol{X}}_c = \boldsymbol{0}, \\ & \boldsymbol{S}_f\left(\boldsymbol{M}\ddot{\boldsymbol{\xi}} + \boldsymbol{h}(\boldsymbol{\xi}, \dot{\boldsymbol{\xi}}) + \boldsymbol{J}_c^T\boldsymbol{f}_{n_c}\right) = \boldsymbol{0}, \\ & |f_{x,y}| \le \mu f_z, \\ & f_z \ge 0. \end{aligned} \tag{34}$$

The objective function is defined based on the task described earlier. The constraints include the acceleration constraints defined in (32) and (33), the constraints imposed by the floating base dynamics, and the friction cone constraints. Here, $\boldsymbol{S}_f$ is a selection matrix that extracts only the components corresponding to the base, $\boldsymbol{M}$ is the inertia matrix, and $\boldsymbol{h}$ represents the combined effects of the centrifugal force vector and the gravity vector. The optimized variables $\ddot{\boldsymbol{\xi}}$ and $\boldsymbol{f}_{n_c}$ obtained from this quadratic programming formulation are then used in an inverse dynamics equation to compute the required torque for each motor.

$$\boldsymbol{\tau}_a = \boldsymbol{S}_a(\boldsymbol{M}\ddot{\boldsymbol{\xi}} + \boldsymbol{h}(\boldsymbol{\xi}, \ddot{\boldsymbol{\xi}}) - \boldsymbol{J}_c^T\boldsymbol{f}_{n_c}). \tag{35}$$

$\boldsymbol{\tau}_a$ and $\boldsymbol{S}_a$ denote the torque of the actuated part and the selection matrix used for actuation, respectively.

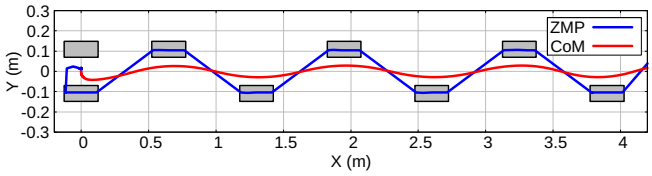

Fig. 9. **Moving ZMP planner in the X-Y plane.** The blue line represents computed ZMP. In the single stance phase, the ZMP moves from the heel to the toe, while in the double stance phase, it shifts from the toe of one foot to the heel of the opposite foot.

VI. Simulation

We validated the proposed heel to toe walking FSM and whole-body controller in simulation using the Qinglong humanoid [19], an adult-scale, full-size platform (height 1.82 m, mass 80 kg) with flat foot measuring 24.6 cm in length. We set the mid-swing height of the swing-foot trajectory to $h_{\text{sw}} = 0.12$ m. The values of the weight matrices used satisfy $\boldsymbol{W}_{reg} \ll \boldsymbol{W}_{up} < \boldsymbol{W}_{\text{sw-IK}} = \boldsymbol{W}_{ap} < \boldsymbol{W}_{CoM}$. The simulations were performed using the MuJoCo [20] physics engine, with quadratic programming solved via qpOASES [21] and the code implemented in C++. The controller operated at a 1 kHz control loop, and all computations and simulations were executed on a PC equipped with an Intel (R) Core(TM) i7-14700KF CPU and 32 GB of RAM. To validate the whole-body controller, we used a moving-ZMP planner based on the LIPM [22], implemented as a receding-horizon MPC to generate CoM/ZMP references. This planner transfers the ZMP from the heel to the toe, making it well-suited for our control scheme. Fig. 9 shows the ZMP trajectory in the X-Y plane as generated by the moving ZMP planner.

A. Joint Torque Requirements in Flat-Foot and Heel to Toe Walking

We compare the performance of conventional flat-foot walking with the proposed knee-stretched heel to toe walking. Fig. 10 shows representative snapshots. The top row depicts conventional flat-foot walking and the bottom row illustrates the proposed knee-stretched heel to toe walking. To ensure a fair comparison we fixed the phase timings to a double-support duration $t_{\text{DSP}} = 0.2$ s and a single-support duration $t_{\text{SSP}} = 0.6$ s, with a commanded step length of 0.72 m. Under these settings the flat-foot gait required lowering the CoM height to 0.82 m to avoid a near-singular configuration at full knee extension. In contrast the heel to toe gait performs heel-off at the stance foot while the swing foot lands with a heel strike. This mechanism enables the same large step at a higher CoM height of 0.98 m. The proposed FSM produces a human-like contact sequence from heel strike through toe-off. Notably, although both the stance and swing legs operate near knee extension, the motion remains smooth and feasible without singularity issues.

Fig. 11 compares the stance-leg knee torque over one step for the two gaits under identical conditions. For flat-foot walking, the peak knee torque is 249.4 N $\cdot$ m and the

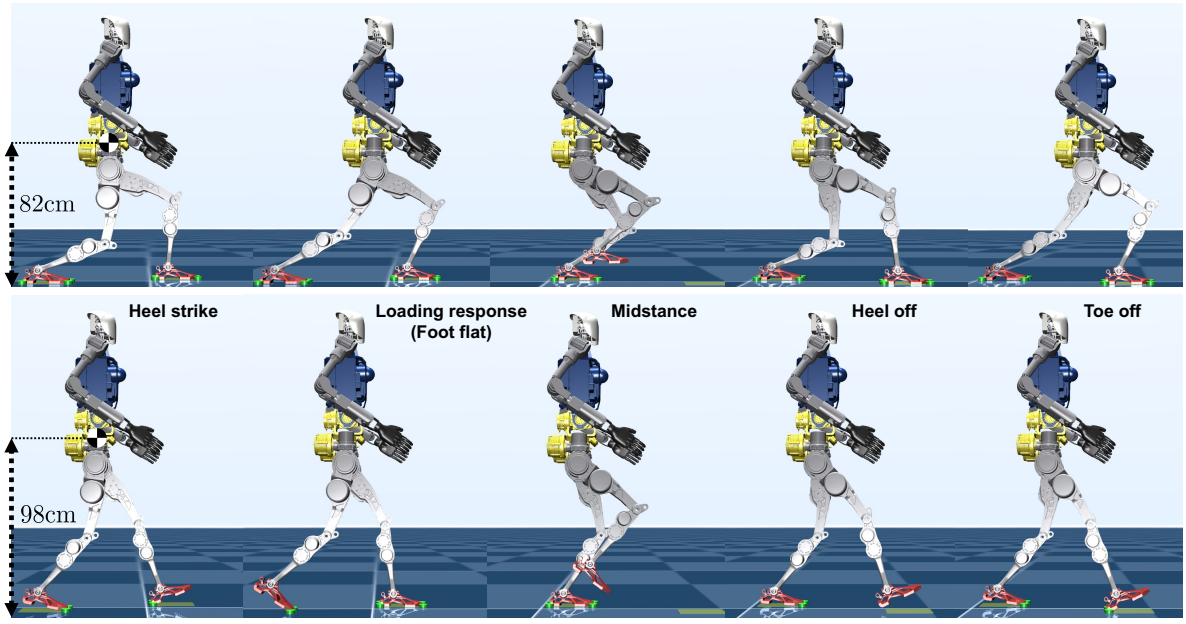

Fig. 10. **Snapshots of conventional flat-foot walking (Top) and the proposed flat-foot heel to toe walking (Bottom).** Each step time remains constant at 0.8 s. The green cylinders in the snapshots indicate the actual contact points between the foot and the ground.

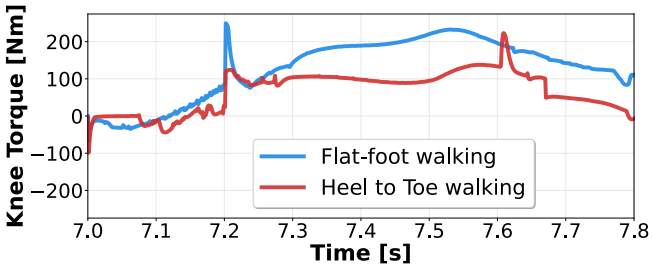

Fig. 11. **Knee torque during large step walking.** Under matched timing and step length, heel to toe reduces overall knee torque compared with flat-foot.

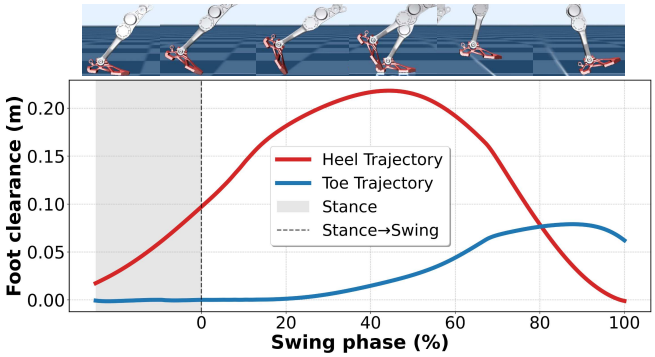

Fig. 12. **Heel and toe clearance over one step.** The grey band indicates stance, and the dashed line marks the stance to swing transition.

mean is 132.6 $\mathrm{N}\cdot\mathrm{m}$. For heel to toe walking, the peak is 233.1 $\mathrm{N}\cdot\mathrm{m}$ and the mean is 72.4 $\mathrm{N}\cdot\mathrm{m}$, indicating that the average torque is reduced by approximately a factor of two. This reduction arises because the flat-foot gait must lower the center of mass to realize the large step length, which in turn forces substantial knee flexion reminiscent of a duck walk. Moreover, the ankle pitch joint must operate at abnormally large angles, often approaching or exceeding the hardware joint limits, which ultimately restricts the attainable step length.

B. Heel and Toe Clearance at Normal-Speed Walking

We evaluate the swing trajectory generated by our controller which combines a 5-DoF Cartesian task for the swing foot with direct ankle pitch joint command at a normal human walking speed. The gait is executed with $t_{\mathrm{SSP}} = 0.40$ s and $t_{\mathrm{DSP}} = 0.10$ s, respectively, and a forward speed of 1.3 m/s. Fig. 12 plots the vertical clearances of the heel and toe relative to the ground plane over one step. During stance, as heel-off develops on the support foot, the heel clearance increases gradually. After toe off (start of swing), both heel and toe clearances rise following the commanded swing profile. Around $\sim 80\%$ of the swing phase the toe clearance overtakes the heel clearance, preparing the foot for a heel-strike landing at the next contact. This temporal ordering and the relative magnitudes of heel and toe clearances are consistent with human heel to toe rollover patterns [23].

C. Heel strike angle versus walking speed (step length)

We fixed the phase timings to $t_{\mathrm{SSP}} = 0.6$ s and $t_{\mathrm{DSP}} = 0.2$ s and varied the desired forward speed v by scaling the step length $L = vT$. The heel strike angle ϕ_{HS} was measured at heel strike. Fig. 13 summarizes the trend. For $v \leq 0.5$ m/s ($L \leq 0.40$ m), ϕ_{HS} stays near zero ($\approx 2.6°$), indicating flat foot touchdown, yet heel off still emerges

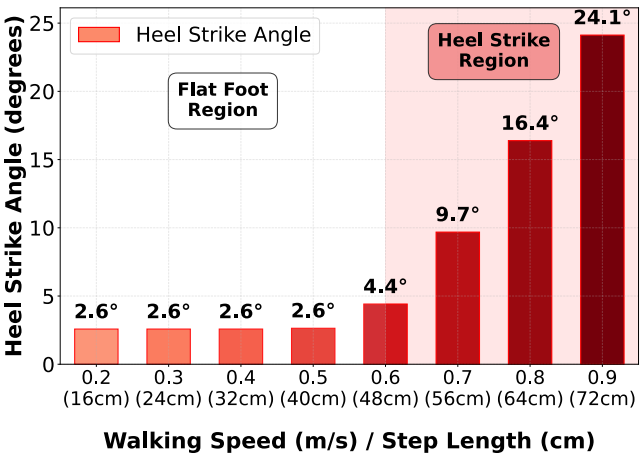

Fig. 13. **Heel–strike angle versus walking speed / step length.** Flat-foot region ($v \leq 0.5$ m/s): $\phi_{\mathrm{HS}} \approx 2.6°$; heel strike region ($v \geq 0.6$ m/s): ϕ_{HS} grows sharply with speed.

naturally during stance. As speed crosses $v \approx 0.6$ m/s ($L \approx 0.48$ m), the late-swing SVA turns positive (Sec. IV-B), and heel-first touchdowns begin to appear. With the ankle-pitch setpoint held constant during late swing, ϕ_{HS} then increases monotonically with speed, reflecting a naturally larger toe-up posture at touchdown.

VII. Conclusion

We presented a hierarchical control framework that achieves human-like heel to toe rollover on flat-foot humanoids. An FSM with mixed time and event based transitions coordinates 5-DoF swing-foot tracking via DLS-IK and a late-swing ankle pitch policy derived from the SVA. A whole-body QP controller enforces phase specific contacts and maintains feasibility near knee extension. In simulation on Qinglong, the method produced longer steps at a higher CoM height with maintained stability and 45% lower mean stance-knee torque, and reproduced human-like heel/toe clearance timing. It also achieved a 72 cm step ($\approx$ 39.6% of height), demonstrating human-level walking performance on a flat-foot humanoid without scripting a heel-strike angle. Future work will extend the approach to uneven terrain and push-recovery and validate it on hardware.

References

[1] David A Winter. *Biomechanics and motor control of human movement*. John wiley & sons, 2009.

[2] Yanshun Zhang, Yingyue Li, Chuang Peng, Dong Mou, Ming Li, and Wei Wang. The height-adaptive parameterized step length measurement method and experiment based on motion parameters. *Sensors*, 18(4):1039, 2018.

[3] M Jacquelin Perry. Gait analysis: normal and pathological function. *New Jersey: SLACK*, 2010.

[4] Yu Ogura, Kazushi Shimomura, Hideki Kondo, Akitoshi Morishima, Tatsu Okubo, Shimpei Momoki, Hun-ok Lim, and Atsuo Takanishi. Human-like walking with knee stretched, heel-contact and toe-off motion by a humanoid robot. In *2006 IEEE/RSJ International Conference on Intelligent Robots and Systems*, pages 3976–3981, 2006.

[5] Shlok Agarwal and Marko Popovic. Study of toe joints to enhance locomotion of humanoid robots. In *2018 IEEE-RAS 18th International Conference on Humanoid Robots (Humanoids)*, pages 1039–1044, 2018.

[6] Mahdokht Ezati, Majid Khadiv, and S. Ali A. Moosavian. Effects of toe-off and heel-off motions on gait performance of biped robots. In *2015 3rd RSI International Conference on Robotics and Mechatronics (ICROM)*, pages 007–012, 2015.

[7] E. Kouchaki and M. J. Sadigh. Effect of toe-joint bending on biped gait performance. In *2010 IEEE International Conference on Robotics and Biomimetics*, pages 697–702, 2010.

[8] Scott Kuindersma, Robin Deits, Maurice Fallon, Andrés Valenzuela, Hongkai Dai, Frank Permenter, Twan Koolen, Pat Marion, and Russ Tedrake. Optimization-based locomotion planning, estimation, and control design for the atlas humanoid robot. *Autonomous robots*, 40:429–455, 2016.

[9] Olivier Stasse, Thomas Flayols, Rohan Budhiraja, Kevin Giraud-Esclasse, Justin Carpentier, Joseph Mirabel, Andrea Del Prete, Philippe Souères, Nicolas Mansard, Florent Lamiraux, et al. Talos: A new humanoid research platform targeted for industrial applications. In *2017 IEEE-RAS 17th International Conference on Humanoid Robotics (Humanoids)*, pages 689–695. IEEE, 2017.

[10] Stéphane Caron, Abderrahmane Kheddar, and Olivier Tempier. Stair climbing stabilization of the hrp-4 humanoid robot using whole-body admittance control. In *2019 International Conference on Robotics and Automation (ICRA)*, pages 277–283, 2019.

[11] Johannes Englsberger, Alexander Werner, Christian Ott, Bernd Henze, Maximo A Roa, Gianluca Garofalo, Robert Burger, Alexander Beyer, Oliver Eiberger, Korbinian Schmid, et al. Overview of the torque-controlled humanoid robot toro. In *2014 IEEE-RAS international conference on humanoid robots*, pages 916–923. IEEE, 2014.

[12] Unitree, "g1," [online]. available: https://www.unitree.com/g1.

[13] Yu-Ming Chen, Gabriel Nelson, Robert Griffin, Michael Posa, and Jerry Pratt. Integrable whole-body orientation coordinates for legged robots. In *2023 IEEE/RSJ International Conference on Intelligent Robots and Systems (IROS)*, pages 10440–10447. IEEE, 2023.

[14] Yixiang Liu, Xizhe Zang, Shuai Heng, Zhenkun Lin, and Jie Zhao. Human-like walking with heel off and toe support for biped robot. *Applied Sciences*, 7(5), 2017.

[15] Beomyeong Park and Jaeheung Park. Heel-strike and toe-off walking of humanoid robot using quadratic programming considering the foot contact states. *Robotics and Autonomous Systems*, 163:104396, 2023.

[16] George Mesesan, Johannes Englsberger, Gianluca Garofalo, Christian Ott, and Alin Albu-Schäffer. Dynamic walking on compliant and uneven terrain using dcm and passivity-based whole-body control. In *2019 IEEE-RAS 19th International Conference on Humanoid Robots (Humanoids)*, pages 25–32, 2019.

[17] Peter Berkelman, Peter Rossi, Timothy Lu, and Ji Ma. Passive orthosis linkage for locomotor rehabilitation. In *2007 IEEE 10th International Conference on Rehabilitation Robotics*, pages 425–431. IEEE, 2007.

[18] Jaeheung Park. *Control Strategies for Robots in Contact*. PhD thesis, Stanford University, 2006.

[19] Ltd Humanoid Robot (Shanghai) Co. OpenLoong-DynamicsControl: Motion control framework of humanoid robot based on MPC and WBC, 2024.

[20] Emanuel Todorov, Tom Erez, and Yuval Tassa. Mujoco: A physics engine for model-based control. In *2012 IEEE/RSJ international conference on intelligent robots and systems*, pages 5026–5033. IEEE, 2012.

[21] Hans Joachim Ferreau, Christian Kirches, Andreas Potschka, Hans Georg Bock, and Moritz Diehl. qpoases: A parametric active-set algorithm for quadratic programming. *Mathematical Programming Computation*, 6:327–363, 2014.

[22] Xuechao Chen, Qiang Huang, Zhangguo Yu, Wei Xu, Jing Li, and Gan Ma. Biped walking planning using extended linear inverted pendulum mode with a continuous moving zmp. In *2011 IEEE International Conference on Mechatronics and Automation*, pages 1280–1285, 2011.

[23] Benoit Mariani, Stephane Rochat, Christophe J Büla, and Kamiar Aminian. Heel and toe clearance estimation for gait analysis using wireless inertial sensors. *IEEE Transactions on Biomedical Engineering*, 59(11):3162–3168, 2012.